[Invited Paper]

Quantifying subcellular dynamics in apoptotic cells with two-dimensional Gabor filters

Robert M. Pasternack, Bryan Rabin, Jing-Yi Zheng, and Nada N. Boustany*

Department of Biomedical Engineering, Rutgers University, Piscataway, NJ 08854, USA
**nboustan@rci.rutgers.edu*

Abstract: We demonstrate an optical Fourier filtering method which can be used to characterize subcellular morphology during dynamic cellular function. In this paper, our Fourier filters were based on two-dimensional Gabor elementary functions, which can be tuned to sense directly object size and orientation. We utilize this method to quantify changes in mitochondrial and nuclear structure during the first three hours of apoptosis. We find that the technique is sensitive to a decrease in particle orientation consistent with apoptosis-induced mitochondrial fragmentation. The scattering signal changes were less pronounced in the nucleus and the remainder of the cytoplasm. Particles in these regions were less oriented than mitochondria and did not change orientation significantly.

OCIS codes: (170.1530) Cell analysis; (070.1170) Analog optical signal processing; (290.5820) Scattering measurements.

References and links

1. D. Hanahan, and R. A. Weinberg, "The hallmarks of cancer," Cell **100**(1), 57–70 (2000).
2. L. Galluzzi, S. A. Aaronson, J. Abrams, E. S. Alnemri, D. W. Andrews, E. H. Baehrecke, N. G. Bazan, M. V. Blagosklonny, K. Blomgren, C. Borner, D. E. Bredesen, C. Brenner, M. Castedo, J. A. Cidlowski, A. Ciechanover, G. M. Cohen, V. De Laurenzi, R. De Maria, M. Deshmukh, B. D. Dynlacht, W. S. El-Deiry, R. A. Flavell, S. Fulda, C. Garrido, P. Golstein, M.-L. Gougeon, D. R. Green, H. Gronemeyer, G. Hajnóczky, J. M. Hardwick, M. O. Hengartner, H. Ichijo, M. Jäättelä, O. Kepp, A. Kimchi, D. J. Klionsky, R. A. Knight, S. Kornbluth, S. Kumar, B. Levine, S. A. Lipton, E. Lugli, F. Madeo, W. Malorni, J.-C. W. Marine, S. J. Martin, J. P. Medema, P. Mehlen, G. Melino, U. M. Moll, E. Morselli, S. Nagata, D. W. Nicholson, P. Nicotera, G. Nuñez, M. Oren, J. Penninger, S. Pervaiz, M. E. Peter, M. Piacentini, J. H. M. Prehn, H. Puthalakath, G. A. Rabinovich, R. Rizzuto, C. M. P. Rodrigues, D. C. Rubinsztein, T. Rudel, L. Scorrano, H.-U. Simon, H. Steller, J. Tschopp, Y. Tsujimoto, P. Vandenabeele, I. Vitale, K. H. Vousden, R. J. Youle, J. Yuan, B. Zhivotovsky, and G. Kroemer, "Guidelines for the use and interpretation of assays for monitoring cell death in higher eukaryotes," Cell Death Differ. **16**(8), 1093–1107 (2009).
3. N. N. Boustany, Y. C. Tsai, B. Pfister, W. M. Joiner, G. A. Oyler, and N. V. Thakor, "BCL-xL-dependent light scattering by apoptotic cells," Biophys. J. **87**(6), 4163–4171 (2004).
4. J. D. Wilson, B. R. Giesselman, S. Mitra, and T. H. Foster, "Lysosome-damage-induced scattering changes coincide with release of cytochrome c," Opt. Lett. **32**(17), 2517–2519 (2007).
5. C. S. Mulvey, A. L. Curtis, S. K. Singh, and I. J. Bigio, "Elastic Scattering Spectroscopy as a Diagnostic Tool for Apoptosis in Cell Cultures," IEEE J. Sel. Top. Quantum Electron. **13**(6), 1663–1670 (2007).
6. K. J. Chalut, J. H. Ostrander, M. G. Giacomelli, and A. Wax, "Light scattering measurements of subcellular structure provide noninvasive early detection of chemotherapy-induced apoptosis," Cancer Res. **69**(3), 1199–1204 (2009).
7. I. Itzkan, L. Qiu, H. Fang, M. M. Zaman, E. Vitkin, I. C. Ghiran, S. Salahuddin, M. Modell, C. Andersson, L. M. Kimerer, P. B. Cipolloni, K.-H. Lim, S. D. Freedman, I. Bigio, B. P. Sachs, E. B. Hanlon, and L. T. Perelman, "Confocal light absorption and scattering spectroscopic microscopy monitors organelles in live cells with no exogenous labels," Proc. Natl. Acad. Sci. U.S.A. **104**(44), 17255–17260 (2007).
8. R. M. Pasternack, Z. Qian, J. Y. Zheng, D. N. Metaxas, E. White, and N. N. Boustany, "Measurement of subcellular texture by optical Gabor-like filtering with a digital micromirror device," Opt. Lett. **33**(19), 2209–2211 (2008).
9. R. M. Pasternack, Z. Qian, J. Zheng, D. N. Metaxas, E. White, and N. N. Boustany, "Measurement of subcellular texture by optical Gabor-like filtering with a digital micromirror device: erratum," Opt. Lett. **34**(13), 1939 (2009).
10. R. M. Pasternack, Z. Qian, J.-Y. Zheng, D. N. Metaxas, and N. N. Boustany, "Highly sensitive size discrimination of sub-micron objects using optical Fourier processing based on two-dimensional Gabor filters," Opt. Express **17**(14), 12001–12012 (2009).

#131132 - $15.00 USD Received 6 Jul 2010; revised 21 Aug 2010; accepted 21 Aug 2010; published 25 Aug 2010

11. J. G. Daugman, "Uncertainty relation for resolution in space, spatial frequency, and orientation optimized by two-dimensional visual cortical filters," J. Opt. Soc. Am. A **2**(7), 1160–1169 (1985).
12. J.-Y. Zheng, R. M. Pasternack, and N. N. Boustany, "Optical Scatter Imaging with a digital micromirror device," Opt. Express **17**(22), 20401–20414 (2009).
13. N. N. Boustany, R. Drezek, and N. V. Thakor, "Calcium-induced alterations in mitochondrial morphology quantified in situ with optical scatter imaging," Biophys. J. **83**(3), 1691–1700 (2002).
14. R. M. Pasternack, J.-Y. Zheng, and N. N. Boustany, "Optical Scatter Changes at the Onset of Apoptosis Are Spatially Associated with Mitochondria," J. Biomed. Opt. In press.
15. A. V. Loud, "A quantitative stereological description of the ultrastructure of normal rat liver parenchymal cells," J. Cell Biol. **37**(1), 27–46 (1968).
16. S. Frank, B. Gaume, E. S. Bergmann-Leitner, W. W. Leitner, E. G. Robert, F. Catez, C. L. Smith, and R. J. Youle, "The role of dynamin-related protein 1, a mediator of mitochondrial fission, in apoptosis," Dev. Cell **1**(4), 515–525 (2001).

1. Introduction

Defects in apoptosis or programmed cell death, contribute to the evolution of many cancers by promoting tumor growth, and conferring resistance to many chemotherapeutic treatments, which function by activation of apoptosis [1]. Assessing apoptosis resistance and its relationship to cancer cell genotype critically depends on the ability to analyze the response of multiple cancer cell types to multiple treatment conditions. Thus methodologies that could rapidly detect the presence of apoptosis could benefit cancer research and treatment by accelerating drug discovery and providing a means to investigate the effect of potential chemotherapeutic agents on cells isolated from biopsies.

Apoptosis is characterized by a sequence of molecular events which result in distinctive morphological changes including nuclear fragmentation, chromatin condensation, and alterations in mitochondrial structure. Standard apoptosis assays rely on assessing more than one marker and typically involve fluorescent labels to identify specific molecular processes in addition to morphological assessment by light microscopy [2]. Electron microscopy is also occasionally used to analyze ultrastructural changes including alterations in organelle morphology, protein localization, and early chromatin condensation [2].

In recent years, several studies have demonstrated the potential use of light scattering methods to monitor subcellular morphology during apoptosis [3–6]. Light scattering methods are advantageous because they are label-free, provide quantitative measures of subcellular morphology, and remain sensitive to ultrastructural changes without having to resort to laborious and costly electron microscopy assays [7]. Here, we present a wide-field optical scatter imaging modality with sensitivity to dynamic alterations in size, shape, and orientation of sub-micron structures to investigate early apoptotic changes. The method utilizes optical Fourier filtering based on tunable Gabor-like filters for their ability to directly characterize object structure in situ and without relying on a predictive scatter model such as Mie theory [8–10]. Using an experimental model consisting of endothelial cells treated with the apoptosis inducer, staurosporine (STS), we apply this method to analyze mitochondrial and nuclear dynamics during the first three hours of apoptosis.

2. Methods

2.1 Optical Fourier filtering of the sample object

The output of a conventional inverted microscope (Carl Zeiss Axiovert 200M) was spatially filtered by a spatial light modulator (SLM, Holoeye Photonics, LC R-2500, or TI 0.7 XGA DMD1100, Texas Instruments) placed in a conjugate Fourier plane (Fig. 1). The spatial frequency resolution on the SLM was 0.0123 cycles/μm/DMD pixel or 0.0068 cycles/μm/LCD pixel with an objective numerical aperture (NA) of 1.4. For weakly scattering aqueous samples, the scattering angle, θ, may be related to spatial frequency, f, by $(n_w \sin\theta)/\lambda = f$. $n_w = 1.33$, and λ was 633nm (helium-neon laser) or 638nm (diode laser). The filtered image stack was collected on a Cascade 512 CCD (Roper Scientific) and analyzed pixel-by-pixel to extract morphometric parameters associated with each pixel. These results are encoded into optically processed images that directly display values of the measured morphometric parameters at each pixel within the field of view (Fig. 1 inset 3). The optically

#131132 - $15.00 USD Received 6 Jul 2010; revised 21 Aug 2010; accepted 21 Aug 2010; published 25 Aug 2010

processed images could be registered with differential interference contrast (DIC) and fluorescence images of the object.

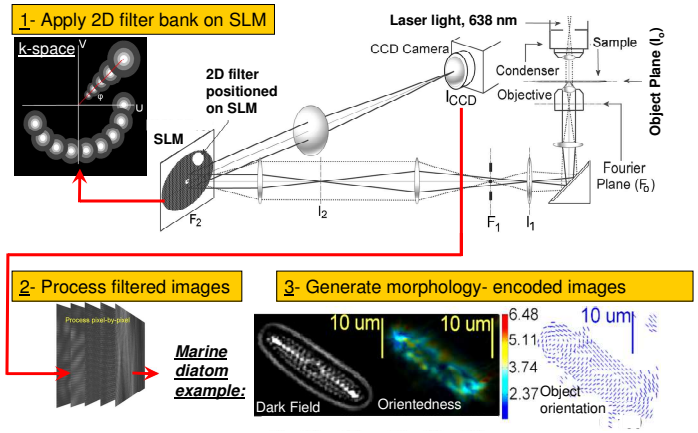

Fig. 1. Optical setup and data processing (set up shown for DMD configuration). The light scattered by the object is Fourier-filtered by a spatial light modulator (SLM in upper left). The stack of filtered images (lower left) collected on the CCD is processed pixel-by-pixel and results in morphometrically encoded images of the object that can be registered directly with other modalities. An example is shown for a marine diatom processed using Gabor filters with constant period and varying orientation. In the "orientedness" image the overall pixel response and the degree of orientation, or aspect ratio, are encoded in the color saturation and hue, respectively. An aspect ratio near 1 (blue) is present in areas in which there is no preferred response angle (low orientedness), while greater values (red) indicate areas in which a higher preferred angle response is present (high orientedness). The orientation of the object features is encoded in a quiver plot (Object orientation image), where each line represents the underlying local feature orientation visible in dark-field. (Adapted from [8])

2.2 Design of optical filters

To characterize scatterer size, orientation and aspect ratio, we implemented two-dimensional (2D) Gabor filter banks on the SLM (inset #1 in Fig. 1). In the space domain, a 2D Gabor filter is composed of a 2D Gaussian multiplied by a complex 2D sinusoid [11]. In Fourier space (on the SLM), the filter corresponds to a single Gaussian-shaped band-pass filter whose center is located at the frequencies (*U, V*) in cycles/μm (Fig. 2). The period and orientation of the sinusoid in the space domain are $S = 1/\sqrt{U^2 + V^2}$, and $\phi = \arctan(V/U)$, respectively, and we set the standard deviation of the Gaussian envelope in object space to σ_s = S/2 (Fig. 2). The Gabor filter half-width in the image plane defines the extent of the object area being analyzed and is inversely proportional to the filter half-width in the Fourier plane. Due to their Gaussian envelope, Gabor filters confine the band-pass filtering to local spatial areas [11].

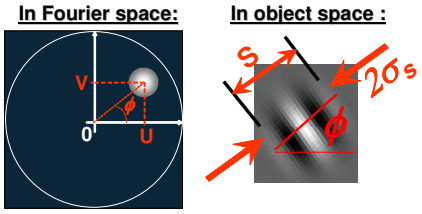

Fig. 2. Gabor filter transform (left) and real part in object space (right).

The Gabor filter response at each position in the object is given by the convolution of the Gabor filter with the object, and is directly obtained in our system by applying the Gabor filter on the SLM while collecting the image of the object on the CCD camera (Fig. 1). A Gabor filter bank is defined by a set of S and ϕ values to analyze local object features. Local features

#131132 - $15.00 USD Received 6 Jul 2010; revised 21 Aug 2010; accepted 21 Aug 2010; published 25 Aug 2010

are described by the Gabor filters which maximize the filtered signal response. As found previously [10,12], if the object's field amplitude or phase profile in space is approximated by a function with width W, and orientation α, the maximum Gabor response was achieved when W was approximately S/2 μm and $\alpha = \phi + \pi/2$. In particular, we had found in [10] that the localized Gabor filters are not only sensitive to infinite periodic patterns, but can also be tuned to sense the diameter of a localized finite object. For finite objects consisting of spheres our results in [10] suggest that a sphere of a given diameter acts roughly like half the period of a periodic pattern. We specifically found that as we varied the Gabor filter period, the optimum Gabor period that gave maximum signal scaled linearly with sphere diameter and the slope of this line was 2.32.

In this study we utilized three filter banks: 1) $0^o \le \phi < 360^o$ in 15° increments at $S = 0.6\mu m, 0.9\mu m, 1.2\mu m, 1.8\mu m, 3.6\mu m$, 2) $S = 0.9\mu m$, and $0^o \le \phi < 180^o$ in 20° increments, 3) $S = 1.8\mu m$, and $0^o \le \phi < 180^o$ in 20° increments. Filterbank 1 was applied with a recently built LCD-based automated system and corresponds to the data in Figs. 3–5; Filterbanks 2 and 3 were applied with the DMD [10] and correspond to the data in Figs. 6 and 7.

2.3 Cell preparation

Bovine aortic endothelial cells (BAEC) were cultured on glass coverslips and labeled with Mitotracker Green (Invitrogen) as previously described [13]. Apoptosis was induced by replacing the viewing medium (Liebowitz L-15 medium + 10% fetal bovine serum) with viewing medium containing 1 μM of the apoptosis inducer staurosporine (STS), obtained from a 4mM STS stock in dimethylsulfoxide (DMSO). Control studies consisted of loading the viewing medium with DMSO only in the same volume in place of the STS solution. Apoptosis of STS-treated endothelial cells was independently confirmed by positive immunofluorescence of activated caspase 3.

2.4 Data acquisition and analysis

Optical filtering was applied for three hours after STS addition at T = 0. At each timepoint, background images of a glass coverslip with no sample were also collected. As described in [14], at each timepoint studied with the Gabor filter technique (for Filterbanks 1 and 2), fluorescent images of the Mitotracker-labeled cells were also acquired with a FITC filter cube (filter No. 10; Carl Zeiss, Gottingen, Germany), and without Fourier spatial filtering, bypassing the DMD by sending the light through the trinocular port of the microscope to a CoolSnap CCD (Roper Scientific). Differential interference images of the cells were acquired on both the CoolSnap and Cascade cameras. This permitted registration of the background-subtracted, dark-field Gabor-filtered images with DIC and fluorescence images. At each pixel we measured the total filter response summed over all angles at each filter period. For each filter period, we also measured the degree of particle orientation, or "orientedness" at each pixel. Orientedness was calculated as the ratio of maximum to average filter response as a function of filter orientation ϕ. For the data collected with ϕ varying over 360° (data in Figs. 4 and 5), orientedness was calculated by taking the average of the centrally-symmetrical maximums over the average filter response as a function of ϕ.

At each timepoint, each cell studied was segmented manually into a region of interest (ROI) and data analysis was confined to these ROIs. As described in [14], the fluorescence images were background corrected to highlight the signal from mitochondria using a *digital* Gabor filter bank with period, S, equivalent to 0.9μm in the object, Gaussian envelope σ_s = S/4 = 0.225 μm, and orientations from 0 to 160° with 20° increments. The Gabor filtered fluorescent images were then summed to yield a background-corrected fluorescent image. Within each ROI we subdivided the cell into three subcellular segments: 1) the nucleus, 2) a region dominated by the bright fluorescently labeled mitochondria 3) the remaining non-fluorescent organelles. First the nucleus was segmented manually guided by the DIC and fluorescence images. Then the remaining cytoplasm region was further segmented into two regions which were segregated using a fluorescence intensity threshold to separate the regions

#131132 - $15.00 USD Received 6 Jul 2010; revised 21 Aug 2010; accepted 21 Aug 2010; published 25 Aug 2010

rich in mitochondria from the remaining non-fluorescent organelles. The threshold was normalized to the average fluorescence intensity within each cell and was set to a value of 0.9 using the thresholding procedure detailed in [14]. We arrived at this value of 0.9 after testing several threshold values and selecting the one that gave the best separation between the signal from mitochondria vs. the remaining non-fluorescent organelles. For example, when the threshold is too low, the designated fluorescent segment above background contains a large fraction of background pixels and its dynamic change in scattering becomes less pronounced. On the other hand, when the threshold is too high, we begin to observe scatter dynamics in the designated background segment since it begins to include fluorescent mitochondria. Using a threshold value of 0.9 we were able to clearly separate the scattering dynamics of fluorescent mitochondria vs. non-fluorescent organelles and used this value in the data shown here. All pixels within each cell ROI were included in this analysis. The three subcellular segments consisting of the nucleus, the bright fluorescent areas rich in mitochondria, and the remaining dim fluorescent areas dominated by other organelles, were separately applied as masks to the optically processed images to compare the changes in filter responses and orientedness within the different subcellular regions.

3. Results and discussion

3.1 Light scattering responses show a loss of organelle orientation during apoptosis

Figure 3 shows unfiltered dark field images of representative cells at T = 0 and 180 min after STS treatment. The images in the lower panels show optically processed images of the same cells. In each of these images, the color brightness encodes the total response (summed over all orientation angles) of the Gabor filters at a given period, S. The color hue encodes the degree of orientation at each Gabor period, taken as the ratio of maximum over average response as a function of orientation angle ϕ. The images show a decrease in orientedness for S = 0.9-1.2 μm.

In Fig. 4 (middle panels) we show quiver plots which encode the local orientation angles of the subcellular structures with responses at S = 0.9 μm. The polar plots (Fig. 4 bottom panels) depict sample Gabor filter responses measured in the cytoplasm and the nucleus of the cells. As can be observed in these examples, the filter responses in the cytoplasm show a preferred angle of orientation, while the responses in the nucleus are more isotropic. The polar plots suggest that in the cytoplasm, the signal from features corresponding to Gabor filter periods of S = 0.6-1.2 μm increases after three hours of apoptosis. At the same time the subcellular particles with responses at S = 0.9 μm become significantly less oriented after the first three hours of apoptosis as also depicted in the quiver plots. On the other hand the signal in the nucleus remains more isotropically distributed and shows stronger responses around values of $S \leq 1.2$. In Fig. 5 the loss of orientedness for S = 0.9 μm is plotted as a function of time for the cells in the field of view.

#131132 - $15.00 USD Received 6 Jul 2010; revised 21 Aug 2010; accepted 21 Aug 2010; published 25 Aug 2010

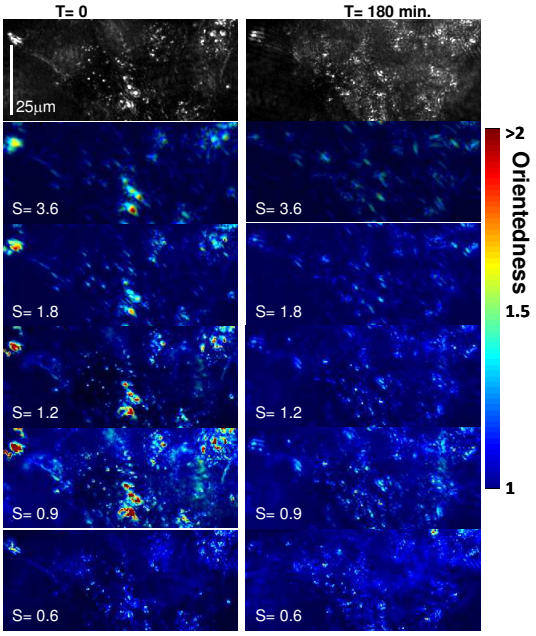

Fig. 3. Dark-field (top panels) and optically processed images of a representative field of view just before and 180 min. after STS treatment. For a given filter period S (in μm), orientedness (colorscale) is taken as the ratio of maximum over average filter response as a function of filter orientation ϕ. The color brightness gives the total response at the filter period, S, summed over all angles.

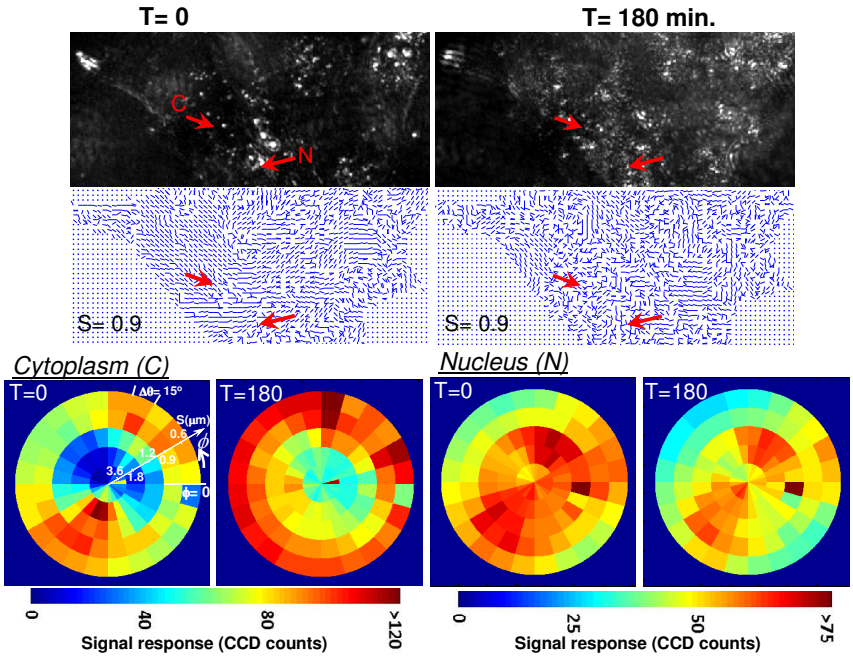

Fig. 4. Dark-field (top panels) and quiver plots (middle panels) showing the orientation angle of subcellular structures with filter responses at S = 0.9 μm. The polar plots show representative data collected with the optical system. Filtered signal responses are shown as a function of filter period S and filter orientation ϕ for two 4x4 pixel regions (arrows) located in the cytoplasm (C) and nucleus (N) just before (T = 0), and 180 min. after STS treatment.

#131132 - $15.00 USD Received 6 Jul 2010; revised 21 Aug 2010; accepted 21 Aug 2010; published 25 Aug 2010

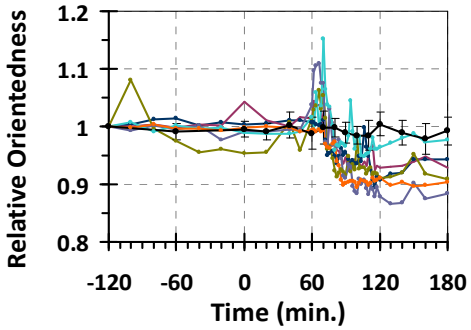

Fig. 5. Average orientedness per cell plotted as a function of time for filter responses at S = 0.9μm. The data were normalized to the value at T = −120min. STS or DMSO was administered at T = 0. Individual traces are shown for the STS-treated cells in the field of view tested in Figs. 3 and 4 (N = 6). The black line with solid black circles is the mean orientedness +/– 95% confidence interval of cells treated with DMSO (N = 7).

3.2 Loss of particle orientation is confined to the mitochondria

As described in Methods, guided by the fluorescence images of the mitochondria and the DIC images of the cells, we studied the optical responses in three subcellular segments consisting of the nucleus, the mitochondria, and the remaining non-fluorescent organelles. In this part of the study we measured Gabor filter responses for S = 0.9μm and S = 1.8 μm at orientations varying between 0° and 160° in 20° increments. Figure 6 depicts the optically processed images of representative cells alongside DIC and fluorescence. The orientedness associated with filter responses at S = 0.9μm decreased after three hours of apoptosis. At the same time mitochondrial fragmentation could be observed in the cells treated with STS. Mitochondrial fragmentation could be observed as early as 60 min after STS addition.

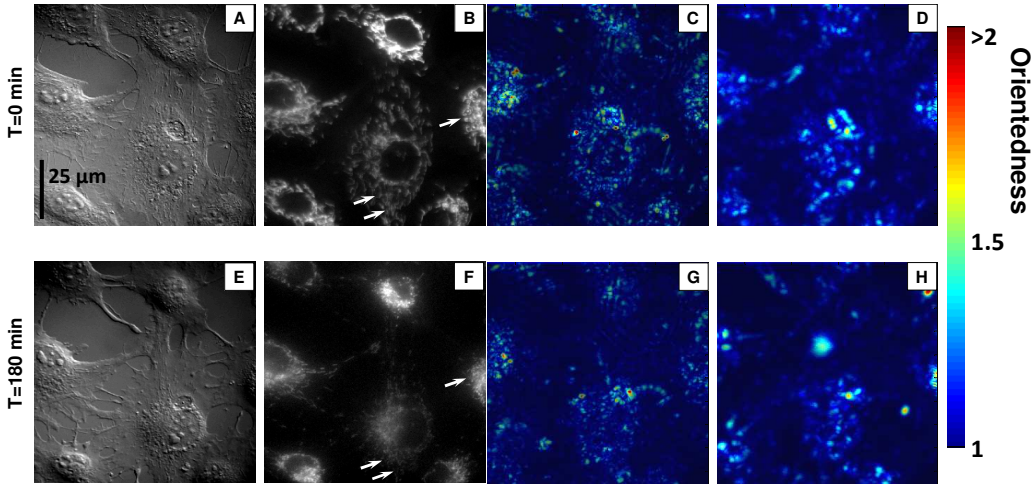

Fig. 6. DIC (A), Mitotracker green fluorescence (B) and response-weighted orientedness images for S = 0.9 μm (C), and S = 1.8 μm (D) right after STS addition at T = 0. E-H: Corresponding imaging modalities at T = 180 min. after STS addition. For a given filter period S, orientedness (color scale) is taken as the ratio of maximum over average filter response as a function of filter orientation ϕ. The color brightness gives the total response at the filter period, S, summed over all angles.

The responses of the individual subcellular regions (Fig. 7) show that there is a 16% increase in signal at S = 0.9 μm beginning at T = 40min, and a 10% increase in signal at S =

#131132 - $15.00 USD Received 6 Jul 2010; revised 21 Aug 2010; accepted 21 Aug 2010; published 25 Aug 2010

1.8 μm beginning right after STS addition at T = 0 in the mitochondrial compartment. There is also an increase in orientedness at T = 40 min. immediately followed by a significant 24% decrease in orientedness in the mitochondrial compartment. These dynamics are absent in the DMSO controls. In contrast, the remaining organelles within the cytoplasm showed no significant change in optical responses or orientedness. In the nucleus, we find that the response at S = 0.9μm increases by 9% within the first 60 minutes and then decreases back to baseline, while the signal at S = 1.8 μm decreases by 13% staring at T = 0 min. Scatterers within the nucleus remain not significantly oriented (orientedness value ~1.2) throughout the first three hours of STS treatment. In general the orientedness of particles with responses at S = 1.8 μm did not significantly change. The mitochondria had a higher response at S = 0.9 μm compared to the remaining organelles in he cytoplasm, and appear to be the main contributor to the scattering responses at S = 0.9μm.

The dynamics reproduce the observations made at the whole cell level (Figs. 3, 5). Importantly, the segmentation of the subcellular regions revealed that the loss of orientation measured in the cytoplasm is spatially confined to regions rich in mitochondria and coincides with mitochondrial fragmentation observed by fluorescence as early as 60 min. after STS addition. In contrast, subcellular particles within the nucleus and the remainder of the cytoplasm start out less oriented than the mitochondria and their degree of orientation does not change significantly.

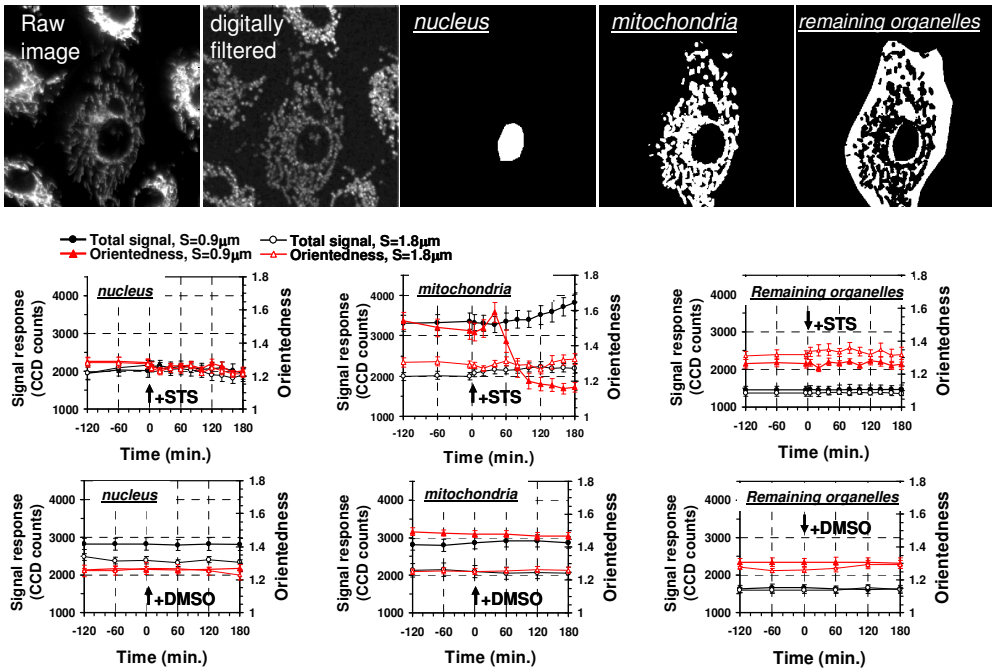

Fig. 7. Top row: Raw and digitally processed fluorescence images of a representative cell shown along the three subcellular segments studied. Middle and bottom rows: In each subcellular compartment, the plots show the total filter response (left axis) at S = 0.9μm (solid black circles) and S = 1.8μm (open circles) summed over all filter orientation angles. Plots of orientedness (right axis) are also shown for S = 0.9 μm (solid red triangles) and S = 1.8μm (open red triangles). Data are mean +/– 95% confidence interval. The mean was calculated by taking the average signal response (or orientedness) per pixel within a given subcellular segment.

We had found that the Gabor filter response are maximized when the diameter of the scatterers correspond to approximately half the Gabor filter period [10]. Thus, particles with a high signal at S = 0.9 μm are approximately 0.45 μm in diameter. This size range corresponds to the reported width of mitochondria between 0.3μm and 0.6 μm [15] and is therefore

#131132 - $15.00 USD Received 6 Jul 2010; revised 21 Aug 2010; accepted 21 Aug 2010; published 25 Aug 2010

consistent with the strong measured response of mitochondria at this spatial frequency. The orientedness dynamics and mitochondrial fragmentation observed in this study corroborate previous reports of mitochondrial fragmentation in apoptotic cells [16]. Interestingly our results also show that orientedness increases immediately before it starts decreasing upon mitochondrial fragmentation. This dynamic could reflect the reported elongation of mitochondria prior to fragmentation [16].

In conclusion the light scattering data measured in this study report on mitochondrial fragmentation early during apoptosis. Further work will be aimed at investigating whether these light scattering changes are correlated with a final commitment to cell death. Light scattering changes resulting from subcellular dynamics later in the apoptotic cascade also remain to be determined by use of the methods presented here. While we have used two-dimensional Gabor filters in this study, other two-dimensional Fourier filtering approaches may also be considered.

Acknowledgments

This study was supported by the National Science Foundation, grant DBI-0852857.

#131132 - $15.00 USD Received 6 Jul 2010; revised 21 Aug 2010; accepted 21 Aug 2010; published 25 Aug 2010